


Article

Very High Cycle Fatigue Life of Free-Spanning Subsea Pipeline Subjected to Vortex-Induced Vibrations

Qingyuan Song^{1,2}, Jun Liu^{1,2} and Fuping Gao^{1,2,*} 

¹ Institute of Mechanics, Chinese Academy of Sciences, Beijing 100190, China; songqingyuan@imech.ac.cn (Q.S.); liujun@imech.ac.cn (J.L.)

² School of Engineering Science, University of Chinese Academy of Sciences, Beijing 100049, China

* Correspondence: fpgao@imech.ac.cn

Abstract: Free-spanning subsea pipelines subjected to vortex-induced vibrations (VIVs) are particularly prone to fatigue failure. Existing flume observations indicated that the VIVs of a near-bed cylinder may be triggered effectively in moderate shear flows. This may imply that the vibration cycles of a spanned pipeline could be up to tens of millions. As such, very high cycle fatigue (VHCF) can occur during engineering service. The free span length is a key parameter for determining the structural natural frequency and the corresponding reduced velocity (V_r). On the basis of the dimensionless vibration amplitude $A/D-V_r$ curve and the recommended S-N curves for high-strength steel pipelines with cathodic protection under seawater environments, a prediction method is proposed for the fatigue life of a free span undergoing VIVs. A parametric study is then performed to evaluate the fatigue life of the spanned pipelines with a focus on VHCF. It is indicated that the minimum fatigue life emerges at certain flow with a moderate velocity for a given span length. With a further decrease or increase in the flow velocity, the fatigue life would be enhanced correspondingly, which could be within the VHCF regime. Such nonlinear variation of the fatigue life with the span length and the flow velocity is attributed to being involved in various VIV branches of the $A/D-V_r$ curve.

Keywords: free-spanning pipeline; vortex-induced vibration; very high cycle fatigue; pipeline–seabed interaction; high-strength steel; seawater environment



Citation: Song, Q.; Liu, J.; Gao, F. Very High Cycle Fatigue Life of Free-Spanning Subsea Pipeline Subjected to Vortex-Induced Vibrations. *J. Mar. Sci. Eng.* **2024**, *12*, 1556. <https://doi.org/10.3390/jmse12091556>

Academic Editor: José António Correia

Received: 31 July 2024

Revised: 23 August 2024

Accepted: 2 September 2024

Published: 5 September 2024



Copyright: © 2024 by the authors. Licensee MDPI, Basel, Switzerland. This article is an open access article distributed under the terms and conditions of the Creative Commons Attribution (CC BY) license (<https://creativecommons.org/licenses/by/4.0/>).

1. Introduction

Subsea pipelines have been widely employed for transporting oil and gas from underwater wells to offshore platforms and onshore processing facilities. The pipeline free-span scenario could be permanent when generated by seabed unevenness, artificial supports for pipeline crossing, or with short-to-long-term evolution by seabed mobility and local scour [1]. Under the action of ocean currents, a partially embedded pipeline may also be suspended because of tunnel erosion [2,3]. As such, free spans are frequently encountered or even inevitable, especially for a long laid pipeline for oil and gas exploitation in deep waters.

In subsea environments, a free-spanning pipeline may suffer from vortex-induced vibrations (VIVs), as illustrated in Figure 1. For an elastically mounted cylinder, the transverse VIVs can be effectively triggered when the reduced velocity (V_r) approaches a critical value $V_{r_{cr}} \approx 4.0$ under wall-free conditions [4]. Once the VIVs are initiated, the frequency of vortex shedding and that of the structural oscillation would collapse into an identical value, which is known as the “lock-in” or “synchronization” phenomenon. The maximum amplitude of the vibration principally depends on the combined mass damping parameter K_s [5]. In engineering practice, subsea pipelines are usually in the proximity of the seabed. For such a near-bed cylinder, the flow fields around the cylinder would be altered due to bed proximity effects, which would subsequently affect the VIV responses. Recently, Liu and Gao [6] investigated the bed proximity effects in triggering

transverse vibration of a cylinder under low K_s conditions. It was found that as the cylinder became closer to the bed boundary (i.e., with a decrease in the gap-to-diameter ratio e/D from 2.0 to 0.1), the values of Vr_{cr} significantly decreased (from 4.0 to 2.85), which was accompanied by a decrease in the vibration amplitudes. Previous flume observations by Gao et al. [7] indicated that once VIVs are triggered, the local scour around the vibrating pipe will be greatly enhanced due to the cyclic vibrations (e.g., the scour depth could be up to approximately $1.2D$, which can be regarded as the wall-free condition for VIV responses).

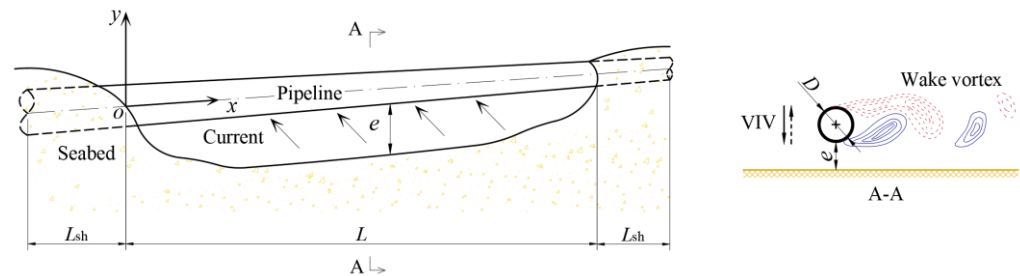


Figure 1. Schematic diagram of a spanning pipeline undergoing VIVs (not in scale).

In engineering practice, fatigue may take place under cyclic loading after a substantial period of service. The fatigue limit stress is generally defined as the highest stress at which specimens do not fail after 10^7 loading cycles. However, the existing studies have extended this knowledge by warning that fatigue failure may occur at lifetimes greater than $N = 10^7$ at a stress which is lower than the conventional fatigue limit [8]. Generally speaking, the fatigue of metallic materials can be divided into three regions: low cycle fatigue (LCF), high cycle fatigue (HCF) and very high cycle fatigue (VHCF), in which the number of cycles to failure is beyond 10^7 . The fatigue behavior in the VHCF region is quite different compared with that in the conventional HCF region [9–13]. For instance, the fatigue behaviors of high-strength steels in the VHCF region show crack initiation at the inclusion site, while in the HCF region, the cracks are located preferentially at the surface [8]. The influence of hydrogen was found to be crucial for eliminating the fatigue limit in the extremely high cycle fatigue region [8,9].

For offshore structures subjected to typical wave and wind loading, significant fatigue failure may occur at $N \geq 10^7$ cycles (i.e., in the VHCF region) [14]. It is also extremely common that turbine blades experience more than $N = 10^7$ stress cycles by vibration. Nevertheless, fatigue test data are normally derived for a number of cycles less than 10^7 , including those for subsea pipeline steels. For the scenario of free-spanning pipelines, the fatigue by VIVs is of great concern in engineering design [15]. The allowable span length of a suspended pipeline was investigated by considering VIV hysteresis effects [16]. The natural frequency of free spans was assessed by using a finite element model [17], and the random ocean current-induced fatigue life of free spans was further predicted on the basis of the Palmgren–Miner cumulative damage rule. Nevertheless, the correlation between the free span length and the corresponding service life has not been understood well, especially in the VHCF region.

In this study, the fatigue life of subsea-spanning pipeline undergoing VIVs is investigated, with a focus on VHCF. Based on the existing flume results for transverse VIV responses, a dimensionless vibration amplitude A/D – Vr curve with four branches is constructed in Section 2.1, and the maximum stress along the free span is then derived in Section 2.2. The bilinear stress range and number of cycles to failure (S–N) curves are recommended by considering the VHCF of high-strength steel pipelines with cathodic protection under seawater environments (see Section 3). Based on the constructed A/D – Vr curve and the recommended S–N curves, a flow chart is proposed in Section 4.1 to predict the fatigue life of a spanning pipeline undergoing VIVs. A parametric study is further performed in Section 4.2 to evaluate the VHCF life of the spanning pipeline. The correlations between

the fatigue life and the flow velocity or the free span length are established. Finally, our concluding remarks are given in Section 5.

2. Vibration Amplitude and Stress Distribution along the Spanning Pipeline

2.1. Amplitude of VIVs

The vibration amplitude is correlated with the reduced velocity Vr , which is defined as

$$Vr = \frac{U}{f_n D} \tag{1}$$

where U is the characteristic velocity of the flow perpendicular to the cylinder's axis; f_n is the structural natural frequency; and D is the outer diameter of the cylinder [4]. The natural frequency (f_n) of a free-spanning pipeline is a key factor in identifying the reduced velocity (see Equation (1)). The natural frequency or the first eigen frequency of a free-spanning pipeline is influenced by many factors (such as the span length, elastic modulus of the pipe steel, boundary conditions, effective mass, and moment of inertia of the pipe), which can be evaluated with the following equation [15]:

$$f_n \approx \frac{C_1}{L_{eff}^2} \left(\frac{(1 + F_{CS})EI}{m_e} \left[1 + \frac{S_{eff}}{P_{cr}} + C_3 \left(\frac{\delta}{D} \right)^2 \right] \right)^{\frac{1}{2}} \tag{2}$$

where L_{eff} is the effective span length; m_e is the effective mass of the pipeline; E is the modulus of elasticity of the steel pipeline; I is the inertia moment of the steel pipeline; S_{eff} is the effective axial force (negative in compression); P_{cr} is the critical buckling load (positive sign); δ is the static deflection; C_1 and C_3 are the end boundary condition coefficients, which depend on the support conditions of the free-span boundary; F_{CS} denotes the stiffness of the concrete coating relative to the steel pipe stiffness; $(1 + F_{CS})$ is the stress concentration factor due to the concrete coating and localized bending; $F_{CS} = k_c \left(\frac{(EI)_{conc}}{EI} \right)^{0.75}$; $(EI)_{conc}$ denotes the stiffness of concrete coating; and the empirical constant k_c accounts for the deformation or slippage in the corrosion coating and the cracking of the concrete coating. With reference to DNV GL [15], the effective span length L_{eff} can be calculated as follows:

$$\frac{L_{eff}}{L} = \begin{cases} \frac{4.73}{-0.066\beta^2 + 1.02\beta + 0.63} & \beta \geq 2.7 \\ \frac{4.73}{0.036\beta^2 + 0.61\beta + 1.0} & \beta < 2.7 \end{cases} \tag{3}$$

In Equation (3), β is the non-dimensional soil stiffness (i.e., $\beta = \log_{10} \left[\frac{KL^4}{(1 + F_{CS})EI} \right]$), where K is the soil stiffness (vertical or horizontal and static or dynamic). The values of β are generally in the range of $2.0 < \beta < 8.0$. For the case of transverse VIV responses, the dynamic vertical stiffness (K_{vd}) can be used (i.e., $K = K_{vd}$), and the following expression can be applied for determination of the dynamic vertical stiffness; that is, $K_{vd} = 0.88G / (1 - \nu)$, where G is the secant shear modulus of soil and ν is the Poisson ratio of the soil [18]. The basic rules for the ideal end conditions are as follows: (1) pinned-pinned, which is used for free spans where each end is allowed to rotate about the pipeline axis, and (2) fixed-fixed, which should be used for free spans which are fixed in place by some sort of anchor at both ends. The following values of C_1 in Equation (2) have been widely used for these typical end conditions: (1) $C_1 = 1.57$ for the pinned-pinned end condition and (2) $C_1 = 3.56$ for the fixed-fixed end condition (see DNV GL [15] and Guo et al. [19]). The effective mass per meter (m_e) is the sum of the mass of the steel pipe per meter (m_p), the mass of the content inside the pipe per meter (m_c), and the added mass per meter (m_a):

$$m_e = m_p + m_c + m_a \tag{4a}$$

$$m_a = C_A \frac{\pi \rho_{water} D^2}{4} \tag{4b}$$

where C_A is the added mass coefficient (for a circular pipeline, $C_A = 1.0$) and ρ_{water} is the density of the seawater. If the effective axial force and the static deflection are not taken into account, then Equation (2) can be simplified as follows:

$$f_n \approx \frac{C_1}{L_{\text{eff}}^2} \left(\frac{(1 + F_{CS})EI}{m_e} \right)^{\frac{1}{2}} \tag{5}$$

In the past few decades, the VIVs of an elastically mounted cylinder have been investigated by quite a few researchers (see the comprehensive reviews of, for example, Williamson and Govardhan [5], Sarpkaya [20], Bearman [21] and Wu et al. [22]). In this study, the VIV amplitudes of wall-free cylinders in the region of the low mass damping parameter K_s (broadly $K_s < 0.05$; see Williamson and Govardhan [5]) were collected from some benchmark flume observations. The whole curve for the nonlinear variation of A/D with Vr was constructed as shown in Figure 2. Note that Wang et al. [23] experimentally studied the VIV of a neutrally buoyant circular cylinder in a recirculating open channel with the mass damping parameter $K_s \approx 3.46 \times 10^{-2}$. In the VIV experiment by de Oliveira Barbosa et al. [24], a freely vibrating cylinder was exposed to currents and placed near a plane boundary parallel to the cylinder axis, and $K_s \approx 1.45 \times 10^{-2}$. Daneshvar and Morton [25] studied the VIV of an elastically mounted circular cylinder in a water tunnel facility, where $K_s \approx 8.32 \times 10^{-3}$. Liu and Gao [6] recently investigated the wall proximity effects on the triggering of transverse VIVs of a circular cylinder with an accessorial low structural damping VIV simulation device, where $K_s \approx 3.14 \times 10^{-2}$. As indicated in Figure 2, in such a low mass damping system, four distinct branches of VIV responses can be identified and marked with various colors, namely the initial excitation branch, the upper branch, the lower branch, and the desynchronization branch (see also Khalak and Williamson [26]). In the initial excitation branch ($3.5 \leq Vr < 5.0$; see Figure 2), the cylinder starts to vibrate with a relatively small amplitude (note: transverse VIVs do not occur at $Vr < 3.5$); in the upper branch ($5.0 \leq Vr < 6.7$), the cylinder vibrates with a large amplitude; in the lower branch ($6.7 \leq Vr < 12$), the cylinder vibrates with a moderate amplitude; and in the desynchronization branch ($Vr \geq 12$), the vibration amplitude of a wall-free circular cylinder is further reduced. There exists a certain dispersion among the experimental data (e.g., at the upper branch; see Figure 2) which could be attributed to involving various values of K_s .

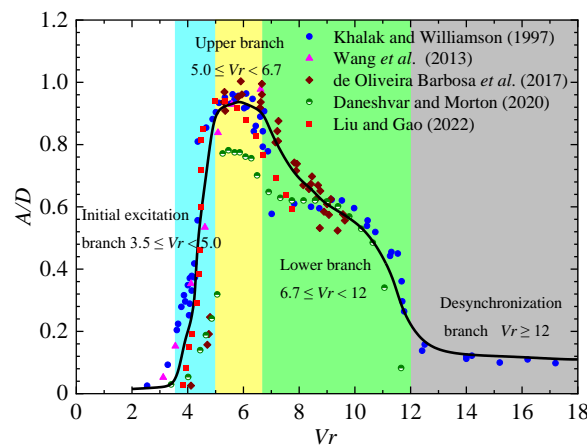


Figure 2. A/D – Vr curve for a wall-free circular cylinder with low mass damping [6,23–26].

The above analyses indicate that once the pipeline parameters and the flow velocity (U) are given, the corresponding reduced velocity (Vr) can be calculated with Equation (1) and Equation (5), and the vibration amplitude can be obtained with reference to Figure 2.

2.2. Stress Distribution along the Free Span

It is supposed that the ocean current is perpendicular to the axis of the free spans, as illustrated in Figure 1. As stated above, the shoulders for a free span can be simplified as the pinned-pinned or fixed-fixed end condition. The maximum deflection in the middle of the span (w_{max}) under the action of a uniform load (q) can be calculated with Equation (6a) for the pinned-pinned end condition and with Equation (6b) for the fixed-fixed end condition [27]:

$$w_{max} = \frac{5qL_{eff}^4}{384EI} \tag{6a}$$

$$w_{max} = \frac{qL_{eff}^4}{384EI} \tag{6b}$$

where L_{eff} is the effective span length. But for the VIV responses, if the maximum deflection w_{max} is given ($w_{max} = A$), then the corresponding maximum bending moment (M_{max}) can be calculated with Equation (7a) for the pinned-pinned end condition and with Equation (7b) for the fixed-fixed end condition [27]:

$$M_{max} = \frac{48EI}{5L_{eff}^2}w_{max} \tag{7a}$$

$$M_{max} = -\frac{32EI}{L_{eff}^2}w_{max} \tag{7b}$$

Figure 3b,c shows the distributions of the bending moment along the free span under these two end conditions. It is indicated that the bending moment reaches its peak value in the middle of the span under the pinned-pinned end condition. But under the fixed-fixed end condition, the two ends connected with the span shoulders undertake the maximum bending moment. Consequently, the maximum normal stresses (σ_{max}) correlated with the maximum deflections (w_{max}) can be expressed as

$$\sigma_{max} = \frac{24DE}{5L_{eff}^2}w_{max} \tag{8a}$$

$$\sigma_{max} = \frac{16DE}{L_{eff}^2}w_{max} \tag{8b}$$

for the pinned-pinned and fixed-fixed end conditions, respectively.

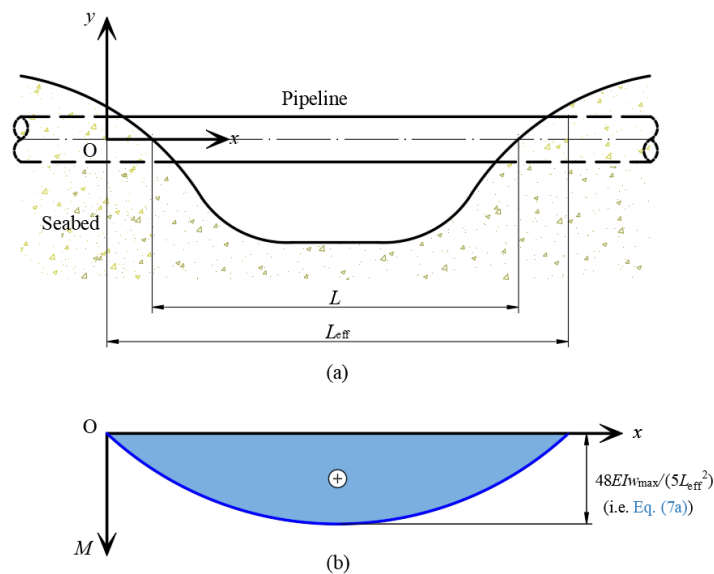


Figure 3. Cont.

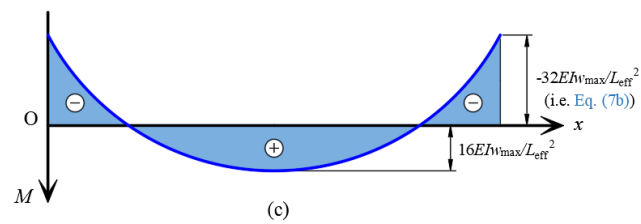


Figure 3. Distributions of bending moment along (a) the spanned pipeline under (b) the pinned-pinned end condition and (c) the fixed-fixed end condition.

3. Recommended S-N Curves

The fatigue design is generally based on the use of S-N curves, which were obtained from fatigue tests. The number of cycles to failure (N) at a stress range ($\Delta\sigma$) is defined by an S-N curve. As mentioned earlier, significant fatigue damage to offshore structures usually occurs at $N \geq 10^7$ cycles (VHCF region). For the VHCF mechanism of metallic materials, a few studies have already been carried out (e.g., Murakami et al. [9], Shiozawa et al. [10], Sakai et al. [28], and Hong et al. [29]). It has been generally recognized that cracks usually initiate from the surface of materials in the LCF and HCF regions, while the cracks preferably emerge in the interior of the materials with a fish eye morphology in the VHCF region. Cracks may initiate from several types of internal defects, which mainly include nonmetallic inclusions, process-related defects, second-phase particles, and microstructural inhomogeneities [30–33]. As illustrated in Figure 4a,b, an inclusion was found at the center of the fish eye zone. The rough area surrounding the inclusion within the fish eye zone, named the fine granular area (FGA), is the crack initiation region, which is critical to VHCF occurrence. The initiation and early growth of cracks could be attributed to the grain refinement caused by the dislocation interaction over a number of cyclic loads followed by the formation of micro-cracks, but the micro-cracks could also form irrespective of the grain refinement during cyclic loading [13].

Submarine pipelines may suffer from corrosion in engineering practices. A distinctive difference between corrosion fatigue and inert environment fatigue is that there is no safe stress range at which metallic materials have infinite fatigue life during engineering service in corrosive environments. The fatigue strength of metallic materials in corrosive environments decreases dramatically for the synergistic interactions between mechanical loading and the environmental effect. Cracks usually occur on the surfaces of metallic materials in very high cycle corrosion fatigue (VHC-CF) [34–37]. The surfaces of metallic materials may be degraded because of corrosion or erosion-corrosion, leading to the formation of pits, grooves, cracks, or rougher surfaces [38]. As illustrated in Figure 4c,d, surface corrosion pits are the origins of cracks for specimens tested in a seawater environment [36,37]. From the microscopic point of view, the corrosive media's attack on the material's surfaces can intensify the formation of microstructurally small cracks (MSCs), contributing to the acceleration of crack initiation and growth. The decrease in metal's ductility or fracture toughness caused by atomic hydrogen is called hydrogen embrittlement (HE), which can make cracks spread quickly with minimal macroscopic signs. In brief, corrosion fatigue is a combination of mechanical and environmental phenomena.

For the sake of service safety, an unfavorable scenario was considered in this case study, such as the weld joint happening to be installed in the middle of the span for the pinned-pinned boundary condition and at one end of the span for the fixed-fixed boundary condition. The service environment was considered to be in the seawater and with cathodic protection (CP).

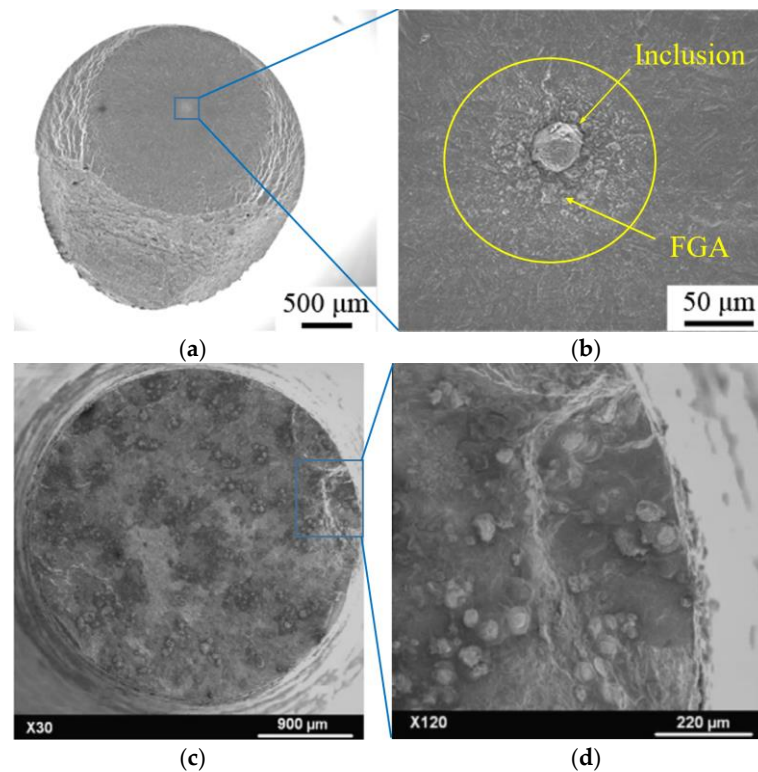


Figure 4. (a) The fracture surface of high-strength steel in an air environment. (b) A close-up of the crack initiation region in (a) [39]. (c) Specimen tested under seawater flow; (d) A close-up of the crack initiation regions in (c) [36].

The fatigue test data were normally derived for a number of cycles less than 10^7 . As such, how to extrapolate the fatigue test data into the VHCF region was important for achieving a reliable assessment procedure [14]. Bilinear S-N curves (i.e., F3 and C1 (see Figure 5)) were recommended to define the number of cycles to failure at a stress range $\Delta\sigma (=2\sigma_{max})$. Note that the F3 curve is for the circumferential butt weld made from one side without a backing bar, and the C1 curve is for the circumferential butt welds made from one side which were machined or ground flush to remove defects and weld overfill [14]. Meanwhile, the existing fatigue test data for the high-strength steels under various environments are also provided in Figure 5 for reference. For the pipe welds with different hot spot geometries, the structural stress concentration factor (SCF) should be accounted for. The SCF is defined as the ratio of local stress (hot spot stress) to nominal stress. It is recommended that $SCF = 1.61$ for the S-N curve F3 and $SCF = 1.0$ for the S-N curve C1 [14]. As shown in Figure 5, the S-N curves in the VHCF region became more horizontal as the number of cycles to failure N became larger than 10^6 . The recommended S-N curves can be expressed in the following form [14]:

$$\text{Log}_{10}(N) = \text{Log}_{10}(\bar{a}) - m\text{Log}_{10}\left(\Delta\sigma\left(\frac{t}{t_{ref}}\right)^k\right) \quad (9)$$

where m is the negative inverse slope of the S-N curve; $\text{Log}_{10}(\bar{a})$ is the intercept of the axis; $\text{Log}_{10}(N)$ is the reference wall thickness of the pipe for welded connections; k is the thickness exponent for the fatigue strength; t is the wall thickness of the pipe; and t_{ref} is the reference wall thickness of the pipe (0.025 m).

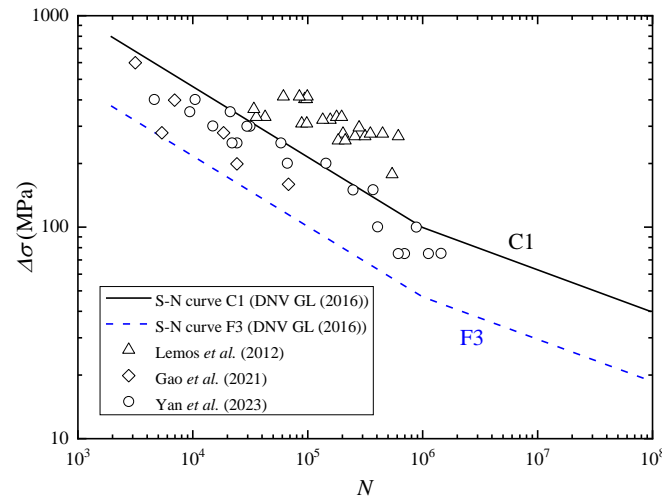


Figure 5. Recommended S-N curves for high-strength steel pipelines in seawater and with cathodic protection (adapted from DNV GL [14]) and the existing test data by Lemos et al. [40] for the saline environments saturated with carbon dioxide, Gao et al. [41] for NACE solution with saturated H₂S, and Yan et al. [42] for the saturated H₂S solution.

4. Fatigue Life Prediction and Discussions

4.1. A Flow Chart for Fatigue Life Prediction

A flow chart is proposed for the fatigue life prediction of a free-spanning pipeline undergoing VIVs, as illustrated in Figure 6. A brief description of the analysis procedure is given below:

- (1) For given structural parameters of the spanned pipeline, the natural frequency (f_n) of the free span can first be evaluated with Equations (2)–(4a). The reduced velocity (Vr) is calculated with Equation (1) for a certain flow velocity (U).
- (2) Once the value of Vr is obtained, the dimensionless vibration amplitude (A/D) can then be evaluated with reference to the recommended A/D – Vr curve (Figure 2). Subsequently, the maximum stress range $\Delta\sigma$ ($= 2\sigma_{\max}$) can be calculated with Equation (8a) or Equation (8b), where the maximum deflection count (w_{\max}) is substituted by the vibration amplitude A .
- (3) By referring to the recommended S-N curves (Figure 5), the fatigue life in terms of the vibration cycles (N) of the spanned pipeline can finally be obtained with Equation (9).

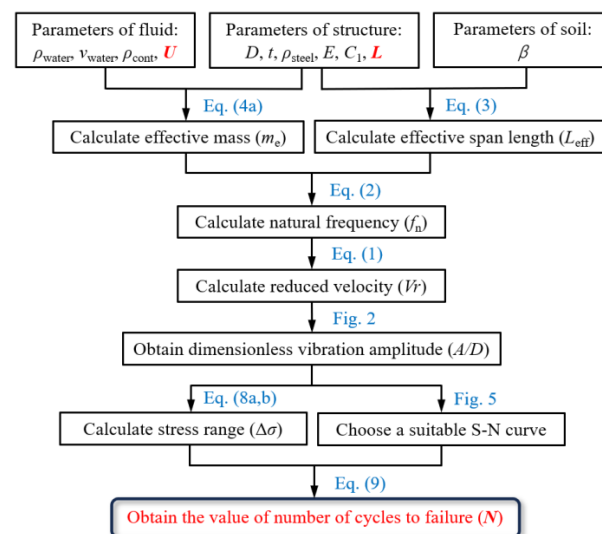


Figure 6. Flow chart for the fatigue life prediction of a free-spanning pipeline undergoing VIVs.

4.2. Parametric Study and Discussions

A subsea pipeline for gas transportation with an outer diameter of 20 inches (0.508 m) was considered for a parametric study. The parameters of the steel pipe, the seawater, the gas inside the pipe, and the soil stiffness are given in Table 1, and the values of the key parameters for the S-N curves are listed in Table 2. For the extreme scenario of large free spans, the span length values (L) were examined in a range from 40 m to 130 m. The correlations between the fatigue life (N) and the flow velocity (U) or span length (L) could be obtained by following the flow chart shown in Figure 6. Table 3 shows the calculation process for the free-spanning pipeline with various values for the span length under the pinned-pinned and the fixed-fixed end conditions. Note that a moderate flow velocity U ($=0.57$ m/s) was considered as an example.

Table 1. Input data for the parameters of the pipe spans.

Parameters	Values	Units
Outer diameter of the steel pipe (D)	0.508	m
Wall thickness of the steel pipe (t)	0.0379	m
Density of the steel (ρ_{steel})	7.870×10^3	kg/m ³
Density of the gas inside the pipe (ρ_{cont})	0.200×10^3	kg/m ³
Density of the seawater (ρ_{water})	1.024×10^3	kg/m ³
Kinematic viscosity of the seawater (ν_{water})	1.565×10^{-6}	m ² /s
Elastic modulus of the steel (E)	2.10×10^{11}	Pa
Moment of inertia of the steel pipe (I)	1.56×10^{-3}	m ⁴
Non-dimensional soil stiffness (β)	4.0	
Reference wall thickness of the pipe (t_{ref})	0.025	m

Table 2. Parameters for the S-N curves.

S-N Curve	$N \leq 10^6$		$N > 10^6$		k
	m_1	$\text{Log}_{10}\left(\frac{-}{a_1}\right)$	m_2	$\text{Log}_{10}\left(\frac{-}{a_2}\right)$	
C1	3	12.049	5	16.081	0.10
F3	3	11.146	5	14.576	0.25

Figure 7a,b illustrates the correlations of the flow velocity (U) and the reduced velocity (Vr) for four selected span length values (i.e., $L = 50$ m, 70 m, 90 m, and 110 m) under the pinned-pinned and fixed-fixed end conditions, respectively. Note that the end condition of the free span had much influence on the natural frequency (f_n) of the free-spanning pipeline, which would further alter the values of Vr (see Equation (1)). As mentioned earlier, the four VIV branches are marked with various colors, which are related to various ranges of Vr (see Figure 2). A shorter free span L would increase the natural frequency f_n (Equation (5)), and thus a higher flow velocity U was required to keep the reduced velocity Vr unchanged (Equation (1)). As indicated in Figure 7, for a given flow velocity U (e.g., $U = 0.57$ m/s; see the horizontal arrow), the corresponding reduced velocity Vr increased with the increase in L .

Table 3. Calculation process for the fatigue life of a free-spanning pipeline with various span length values ($U = 0.57$ m/s).

L (m)	L_{eff} (m)	C1		f_n (Hz)		V_r		A/D		w (m)		σ_{max} (MPa)		N (Predicted with S-N Curve C1)		N (Predicted with S-N Curve F3)	
		P-P	F-F	P-P	F-F	P-P	F-F	P-P	F-F	P-P	F-F	P-P	F-F	P-P	F-F	P-P	F-F
40	51.78	1.57	3.56	0.407	0.916	2.76	1.23	0.019	0	0.010	0	1.82	0	1.52×10^{13}		3.49×10^{11}	
45	58.25	1.57	3.56	0.322	0.724	3.49	1.55	0.025	0	0.013	0	1.95	0	1.07×10^{13}		2.46×10^{11}	
50	64.72	1.57	3.56	0.261	0.586	4.31	1.91	0.410	0	0.208	0	25.44	0	2.87×10^7		7.78×10^5	
55	71.19	1.57	3.56	0.215	0.484	5.21	2.32	0.922	0.017	0.468	0.008	47.30	2.84	1.29×10^6	1.67×10^{12}	1.21×10^5	3.81×10^{10}
60	77.66	1.57	3.56	0.181	0.407	6.20	2.76	0.926	0.019	0.471	0.010	39.95	2.70	3.01×10^6	2.13×10^{12}	2.01×10^5	4.88×10^{10}
65	84.14	1.57	3.56	0.154	0.347	7.28	3.24	0.788	0.023	0.400	0.012	28.95	2.77	1.50×10^7	1.86×10^{12}	5.28×10^5	4.26×10^{10}
70	90.61	1.57	3.56	0.133	0.299	8.44	3.75	0.658	0.103	0.334	0.053	20.86	10.92	7.74×10^7	1.97×10^9	1.77×10^6	4.51×10^7
75	97.08	1.57	3.56	0.116	0.261	9.69	4.31	0.571	0.413	0.290	0.210	15.75	37.97	3.16×10^8	3.88×10^6	7.22×10^6	2.34×10^5
80	103.55	1.57	3.56	0.102	0.229	11.02	4.90	0.438	0.871	0.223	0.443	10.63	70.46	2.26×10^9	3.53×10^5	5.16×10^7	3.66×10^4
85	110.02	1.57	3.56	0.090	0.203	12.44	5.53	0.157	0.928	0.080	0.472	3.37	66.49	7.01×10^{11}	4.20×10^5	1.60×10^{10}	4.36×10^4
90	116.50	1.57	3.56	0.080	0.181	13.95	6.20	0.124	0.926	0.063	0.471	2.37	59.17	4.06×10^{12}	5.96×10^5	9.28×10^{10}	6.18×10^4
95	122.97	1.57	3.56	0.072	0.162	15.54	6.91	0.120	0.857	0.061	0.435	2.06	49.12	8.24×10^{12}	1.07×10^6	1.88×10^{11}	1.08×10^5
100	129.44	1.57	3.56	0.065	0.147	17.22	7.66	0.111	0.727	0.057	0.369	1.73	37.61	1.98×10^{13}	4.07×10^6	4.53×10^{11}	2.41×10^5
105	135.91	1.57	3.56	0.059	0.133	18.99	8.44		0.658		0.334		30.89		1.09×10^7		4.34×10^5
110	142.38	1.57	3.56	0.054	0.121	20.84	9.27		0.592		0.301		25.34		2.93×10^7		7.87×10^5
115	148.86	1.57	3.56	0.049	0.111	22.78	10.13		0.548		0.278		21.44		6.75×10^7		1.54×10^6
120	155.33	1.57	3.56	0.045	0.102	24.80	11.03		0.437		0.222		15.72		3.19×10^8		7.30×10^6
125	161.80	1.57	3.56	0.042	0.094	26.91	11.96		0.225		0.114		7.45		1.34×10^{10}		3.05×10^8
130	168.27	1.57	3.56	0.039	0.087	29.11	12.94		0.142		0.072		4.35		1.97×10^{11}		4.52×10^9

Note: "P-P" is the abbreviation for the "pinned-pinned" end condition, and "F-F" is the abbreviation for the "fixed-fixed" end condition.

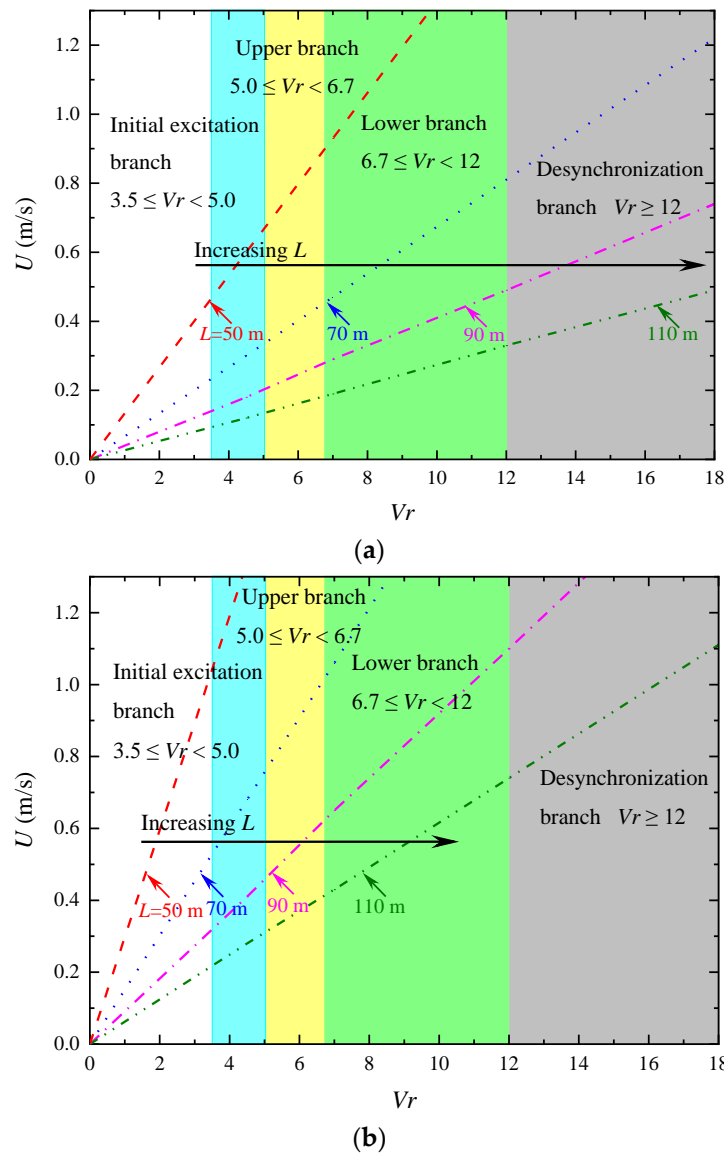


Figure 7. Illustration for VIV branch variations with flow velocities (U) for four selected span length values ($L = 50$ m, 70 m, 90 m, and 110 m) under (a) the pinned-pinned end condition and (b) the fixed-fixed end condition. (Input data for the parameters of the pipe spans are given in Table 1).

The variations in the predicted fatigue life (N) for two recommended S-N curves (see Figure 5) with a span length L at a given flow velocity $U = 0.57$ m/s are presented in Figure 8. Both the pinned-pinned and fixed-fixed end conditions were taken into account. It is indicated that the relationships between the fatigue life N and the span length L under a given flow velocity U were essentially nonlinear. As depicted in Figure 8, for $45 \leq L < 54$ (m) under the pinned-pinned end condition or $68 \leq L < 81$ (m) under the fixed-fixed end condition, the free span vibrated in the initial excitation branch (marked in blue; see Figure 8) such that the fatigue life N decreased with an increase in the span length L . For the span length $54 \leq L < 62$ (m) (pinned-pinned) or $81 \leq L < 94$ (m) (fixed-fixed), the free span vibrated in the upper branch (yellow) with larger amplitudes such that the corresponding fatigue life first became shorter to a minimum value and then increased with the increase in L . But for $62 \leq L < 83$ (m) (pinned-pinned) or $94 \leq L < 125$ (m) (fixed-fixed), the free span vibrated in the lower branch (green) (i.e., the vibration amplitudes were reduced). Therefore, the fatigue life became longer with an increasing L , and for $L \geq 83$ (m) (pinned-pinned) or $L \geq 125$ (m) (fixed-fixed), the free span vibrated in the desynchronization branch (gray) (i.e., the vibration amplitude continued to decrease with

an increasing L) such that the fatigue life became much larger or even $N > 10^8$. From Figure 8a,b, it can be recognized that the critical values of the span length to differentiate the four VIV branches under the pinned-pinned end condition were much smaller than those under the fixed-fixed end condition. This was due to the fact that for a specified value of L , the natural frequency f_n for the pinned-pinned end condition was much smaller than that for the fixed-fixed end condition. As such, to keep the natural frequency f_n unchanged (or the reduced velocity Vr unchanged for a certain flow velocity U ; see Equation (1)), a shorter span length L under the pinned-pinned end condition was required than that under the fixed-fixed end condition.

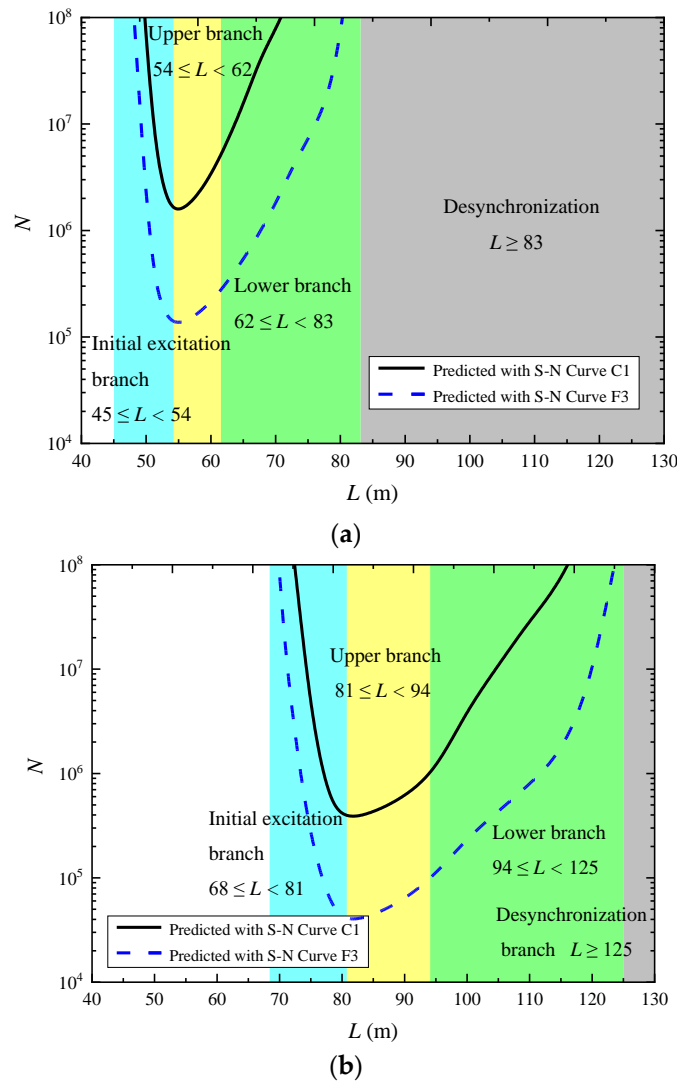
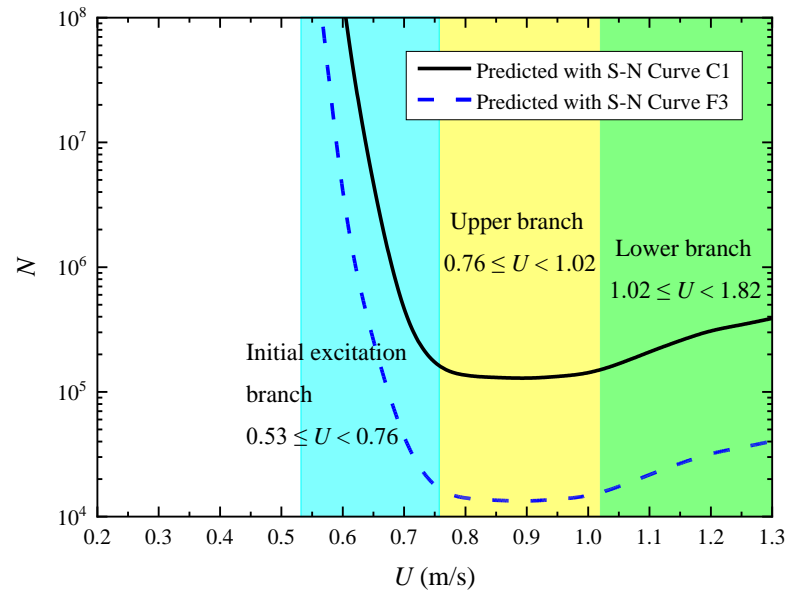


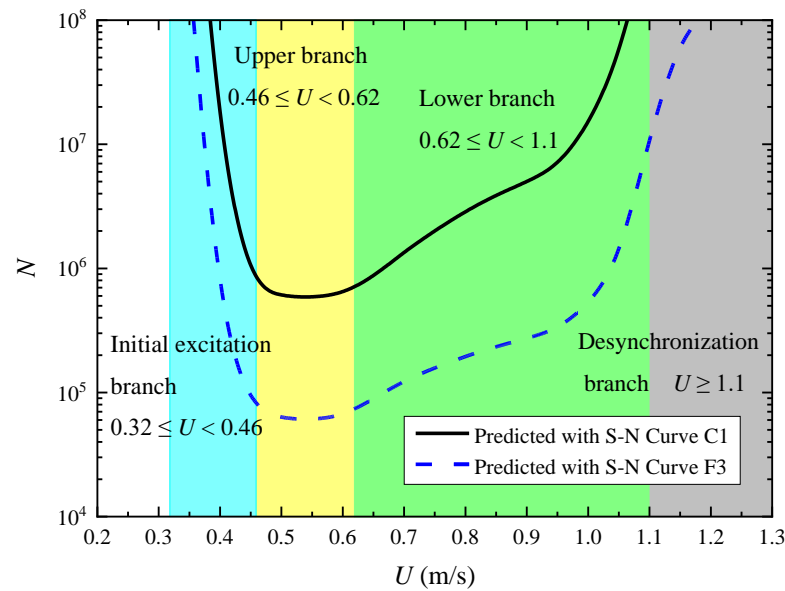
Figure 8. Variations in number of cycles to failure (N) with the span length (L) for the specified flow velocity value ($U = 0.57$ m/s): (a) pinned-pinned end condition and (b) fixed-fixed end condition.

The effect of the flow velocity (U) on the fatigue life (N) was further investigated. The variations in the fatigue life N with the flow velocity U for three span length values $L = 70$ m, 90 m, and 110 m are shown in Figure 9a–c, respectively. If the free span vibrated in the initial excitation branch ($3.5 \leq Vr < 5.0$) (i.e., $0.53 \leq U < 0.76$ (m/s) for $L = 70$ m (Figure 9a), $0.32 \leq U < 0.46$ (m/s) for $L = 90$ m (Figure 9b), and $0.22 \leq U < 0.31$ (m/s) for $L = 110$ m (Figure 9c)), then the fatigue life N decreased with the increase in the flow velocity U . If the free span vibrated in the upper branch with large amplitudes ($5.0 \leq Vr < 6.7$) (i.e., $0.76 \leq U < 1.02$ (m/s) for $L = 70$ m (Figure 9a), $0.46 \leq U < 0.62$ (m/s) for $L = 90$ m (Figure 9b), and $0.31 \leq U < 0.41$ (m/s) for $L = 110$ m (Figure 9c)), then the fatigue life N was first reduced slightly to a minimum value and then gradually increases with an increasing

U . In the lower branch of VIVs ($6.7 \leq Vr < 12$) (i.e., $1.02 \leq U < 1.82$ (m/s) for $L = 70$ m (Figure 9a), $0.62 \leq U < 1.10$ (m/s) for $L = 90$ m (Figure 9b), and $0.41 \leq U < 0.74$ (m/s) for $L = 110$ m (Figure 9c)), the free span vibrated with moderate amplitudes, and the corresponding fatigue life N became longer with the increase in U . Similarly, in the desynchronization branch ($Vr \geq 12$) (i.e., $U > 1.10$ (m/s) for $L = 90$ m (Figure 9b) and $U > 0.74$ (m/s) for $L = 110$ m (Figure 9c)), the free span vibrated with much smaller amplitudes, and the fatigue life N further became longer with the increase in U . It should be noted that for $L = 70$ m (Figure 9a), the desynchronization branch of VIVs was not involved in the examined range of $U < 1.3$ m/s.



(a)



(b)

Figure 9. Cont.

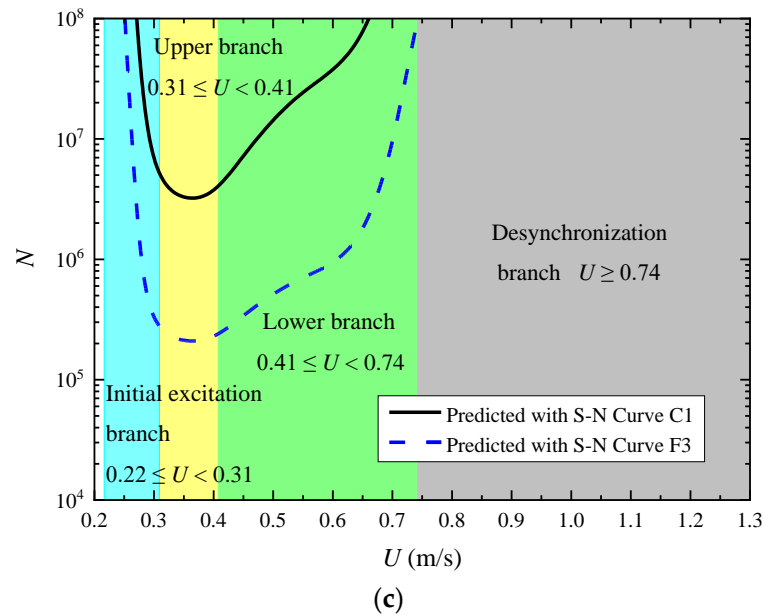


Figure 9. Variations in number of cycles to failure (N) with flow velocity (U) for three selected span length values: (a) $L = 70$ m; (b) $L = 90$ m; and (c) $L = 110$ m.

The above parametric study shows that the fatigue life (N) of the free spans of subsea pipelines is quite sensitive to the span length (L) and the flow velocity (U). By following the flow chart for fatigue life prediction (Section 4.1), the variations in N with U and L could be obtained, as shown in Figure 10. Note that the S-N curve C1 (see Figure 5) was adopted to predict the fatigue life N of the extreme scenario of large free spans. As illustrated by the two-dimensional contour map (Figure 10), for the span length range $70 \leq L \leq 110$ (m) and the flow velocity range $0.2 \leq U \leq 1.3$ (m/s), the minimum value of N ($\approx 1.28 \times 10^5$) emerged at $U \approx 0.9$ m/s for $L = 70$ m (see also Figure 9a). With a further decrease or increase in U for a specified span length value (L), the fatigue life N would be remarkably enhanced, which could be within the regime of very high cycle fatigue (VHCF) (i.e., $N > \sim 10^7$; see Figure 10). As discussed above, such nonlinearity of the relationship between the fatigue life (N) and the flow velocity (U) and span length (L) is mainly attributed to the intrinsic characteristics of VIVs (see Figure 2) (i.e., the nonlinear variation in the dimensionless vibration amplitude with the reduced velocity).

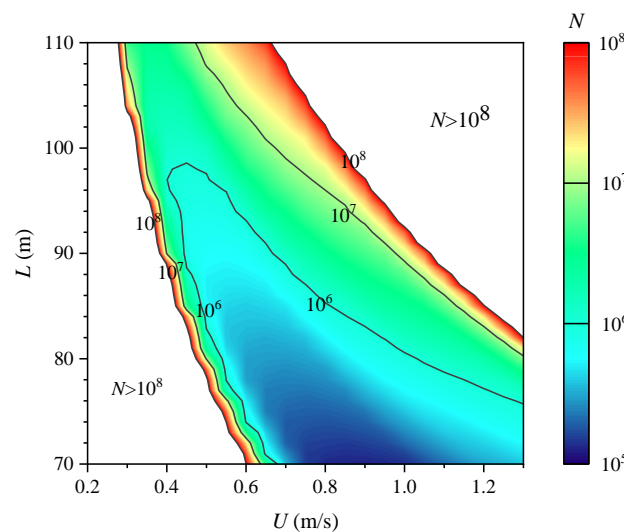


Figure 10. Variations in the number of cycles to failure (N) with flow velocity (U) and span length (L). (Input data for the related pipe span parameters are listed in Tables 1 and 2).

5. Concluding Remarks

In subsea environments, free-spanning subsea pipelines may suffer from vortex-induced vibrations (VIVs), which could further result in fatigue failure after a substantial period of service. In this study, the fatigue failure of free spans caused by VIVs was investigated, with a focus on very high cycle fatigue (VHCF) in the extreme scenario of large free spans under flows with moderate velocities. The following conclusions can be drawn:

- (1) With reference to the benchmark flume observations of the VIV response amplitudes of a low mass damping system, the whole curve for the nonlinear variation in A/D with Vr ($A/D-Vr$ curve) is recommended, in which four distinct branches of VIV responses can be identified (i.e., the initial excitation branch, the upper branch, the lower branch, and the desynchronization branch). Bilinear S-N curves were chosen to describe the relationship between the stress range and the fatigue life of the free spans in a complex seawater environment.
- (2) On the basis of the recommended $A/D-Vr$ curve and the S-N curve for VHCF of high-strength steel in seawater and with cathodic protections, a prediction method was proposed for the fatigue life of free spans undergoing VIVs. If the pipeline and environmental parameters are given, then the fatigue life in terms of the number of cycles to failure N can be evaluated by following the flow chart.
- (3) The nonlinear relationships between the fatigue life N and the flow velocity U and span length L were obtained in a parametric study. For the examined range of span lengths and flow velocities, the minimum fatigue life emerged at a certain flow with a moderate velocity for a given span length L . With a further decrease or increase in U , the fatigue life N would be enhanced correspondingly, which could be within the regime of VHCF. Such nonlinearity of the relationship of N with U and L is mainly attributed to the intrinsic characteristics of VIVs (i.e., the nonlinear variation in the dimensionless vibration amplitude with a reduced velocity).

In the present investigation, a quantitative correlation was established between the VHCF life of a spanning pipeline undergoing VIVs and the key influential parameters (i.e., the span length and the flow velocity). The VHCF life of a spanning pipeline was examined under two extreme (F-F and P-P) end conditions by taking into account the effective span length. This study may provide an instructive reference or methodology for evaluating the service life of subsea-spanning pipelines. It should be noted that the above conclusions are predominantly limited to the engineering scenario of an isolated single span on a relatively flat seabed. Much uncertainty still exists for accurate prediction of the fatigue life of free spans (e.g., the complex pipe–soil interaction at the span shoulders), which needs to be further investigated.

Author Contributions: Conceptualization, F.G.; experiments and data analyses, Q.S. and J.L.; writing—original draft, Q.S.; validation, J.L. and F.G.; review and editing, F.G. and J.L. All authors have read and agreed to the published version of the manuscript.

Funding: This work was funded by the National Natural Science Foundation of China (Grant Nos. 12061160463 and 11825205).

Institutional Review Board Statement: Not applicable.

Informed Consent Statement: Not applicable.

Data Availability Statement: The data presented in this study are available upon request from the corresponding author.

Conflicts of Interest: The authors declare no conflicts of interest.

Notations

A	Vibration amplitude of the cylinder
\bar{a}	Coefficient in Equation (9)
\bar{a}_1	Parameter for the S-N curve in Table 2
\bar{a}_2	Parameter for the S-N curve in Table 2
C_1	Boundary condition coefficient in Equation (2)
C_3	Boundary condition coefficient in Equation (2)
C_A	Added mass coefficient
D	Outer diameter of the cylinder or the pipe
D_i	Inner diameter of the pipe
e	Gap between the pipe's bottom and the seabed surface
E	Elastic modulus of the pipe
$(EI)_{\text{conc}}$	Stiffness of concrete coating
F_{CS}	Concrete stiffness enhancement factor for the pipe
f_n	Natural frequency of the pipe or the cylinder
f_v	Frequency of vortex shedding from a fixed cylinder
G	Shear modulus of the soil
I	Moment of inertia
k	Exponent of thickness of the pipe
k_c	Empirical constant
K	Soil stiffness
K_s	Combined mass damping parameter
K_{vd}	Dynamic vertical stiffness of the soil
L	Free span length of the pipeline
L_{eff}	Effective span length of the pipeline
M	Bending moment of the pipeline
m_1	Parameter for the S-N curve in Table 2
m_2	Parameter for the S-N curve in Table 2
m_a	Added mass of the pipeline per meter
m_c	Mass of the content inside the pipeline per meter
m_e	Effective mass of the pipeline per meter
m_p	Mass of the steel pipeline per meter
N	Number of cycles to fatigue failure
P_{cr}	Critical buckling load
q	Uniform load on the pipeline
SCF	Stress concentration factor
S_{eff}	Effective axial force along the pipeline
t	Wall thickness of the pipe
t_{ref}	Reference wall thickness of the pipe
U	Flow velocity
Vr	Reduced velocity
Vr_{cr}	Critical reduced velocity
w	Deflection of the suspended pipeline
w_{max}	Maximum deflection of the suspended pipeline
β	Non-dimensional soil stiffness
δ	Static deflection of the pipeline
$\Delta\sigma$	Stress range
ρ_{steel}	Density of the steel
ρ_{water}	Density of the seawater
σ	Normal stress
σ_{max}	Maximum normal stress
ν_{water}	Kinematic viscosity of the seawater
ν	Poisson ratio of the soil

References

- Drago, M.; Mattioli, M.; Bruschi, R.; Vitali, L. Insights on the design of free spanning pipelines. *Philos. Trans. R. Soc. A* **2015**, *373*, 20140111. [[CrossRef](#)]
- Sumer, B.M.; Jensen, H.R.; Mao, Y.; Fredsøe, J. Effect of lee-wake on scour below pipelines in current. *J. Waterw. Port Coast. Ocean Eng.* **1988**, *114*, 599–614. [[CrossRef](#)]
- Gao, F.P. Flow-pipe-soil coupling mechanisms and predictions for submarine pipeline instability. *J. Hydrodyn.* **2017**, *29*, 763–773. [[CrossRef](#)]
- Blevins, R.D. *Flow-Induced Vibration*, 2nd ed.; Krieger Publishing Company: New York, NY, USA, 1990.
- Williamson, C.H.K.; Govardhan, R. Vortex-induced vibrations. *Annu. Rev. Fluid Mech.* **2004**, *36*, 413–455. [[CrossRef](#)]
- Liu, J.; Gao, F.P. Triggering mechanics for transverse vibrations of a circular cylinder in a shear flow: Wall-proximity effects. *J. Fluids Struct.* **2022**, *108*, 103423. [[CrossRef](#)]
- Gao, F.P.; Yang, B.; Wu, Y.X.; Yan, S.M. Steady currents induced seabed scour around a vibrating pipeline. *Appl. Ocean Res.* **2006**, *28*, 291–298. [[CrossRef](#)]
- Sharma, A.; Oh, M.C.; Ahn, B. Recent advances in very high cycle fatigue behavior of metals and alloys—A review. *Metals* **2020**, *10*, 1200. [[CrossRef](#)]
- Murakami, Y.; Nomoto, T.; Ueda, T.; Murakami, Y. On the mechanism of fatigue failure in the superlong life regime ($N > 10^7$ cycles). Part I: Influence of hydrogen trapped by inclusions. *Fatigue Fract. Eng. Mater. Struct.* **2000**, *23*, 893–902. [[CrossRef](#)]
- Shiozawa, K.; Lu, L.; Ishihara, S. S-N curve characteristics and subsurface crack initiation behaviour in ultra-long life fatigue of a high carbon-chromium bearing steel. *Fatigue Fract. Eng. Mater. Struct.* **2001**, *24*, 781–790. [[CrossRef](#)]
- Sakai, T.; Sato, Y.; Oguma, N. Characteristic S-N properties of high-carbon-chromium-bearing steel under axial loading in long-life fatigue. *Fatigue Fract. Eng. Mater. Struct.* **2002**, *25*, 765–773. [[CrossRef](#)]
- Hong, Y.; Zhao, A.; Qian, G.; Zhou, C. Fatigue strength and crack initiation mechanism of very-high-cycle fatigue for low alloy steels. *Metall. Mater. Trans. A* **2012**, *43*, 2753–2762. [[CrossRef](#)]
- Song, Q.Y.; Sun, C.Q. Mechanism of crack initiation and early growth of high strength steels in very high cycle fatigue regime. *Mater. Sci. Eng. A* **2020**, *771*, 138648. [[CrossRef](#)]
- Det Norske Veritas and Germanischer Lloyd (DNV GL). *DNVGL-RP-C203: Fatigue Design of Offshore Steel Structures*; DNV: Oslo, Norway, 2016.
- Det Norske Veritas and Germanischer Lloyd (DNV GL). *DNVGL-RP-F105: Free Spanning Pipelines*; DNV: Oslo, Norway, 2017.
- Liu, J.; Gao, F.P. Evaluation for allowable span length of a submarine pipeline considering VIV hysteresis effect. *Int. J. Offshore Polar Eng.* **2021**, *31*, 325–332. [[CrossRef](#)]
- He, Z.F.; Wei, Y.; Liu, S.L. Analysis of safe span length and fatigue life of submarine pipelines. *China Ocean Eng.* **2020**, *34*, 119–130. [[CrossRef](#)]
- Det Norske Veritas and Germanischer Lloyd (DNV GL). *DNVGL-RP-F114: Pipe-Soil Interaction for Submarine Pipelines*; DNV: Oslo, Norway, 2017.
- Guo, B.; Song, S.; Ghalambor, A.; Lin, T.R. *Offshore Pipelines: Design, Installation, and Maintenance*, 2nd ed.; Gulf Professional Publishing: Waltham, MA, USA, 2014.
- Sarpkaya, T. A critical review of the intrinsic nature of vortex-induced vibrations. *J. Fluids Struct.* **2004**, *19*, 389–447. [[CrossRef](#)]
- Bearman, P.W. Circular cylinder wakes and vortex-induced vibrations. *J. Fluids Struct.* **2011**, *27*, 648–658. [[CrossRef](#)]
- Wu, X.; Ge, F.; Hong, Y. A review of recent studies on vortex-induced vibrations of long slender cylinders. *J. Fluids Struct.* **2012**, *28*, 292–308. [[CrossRef](#)]
- Wang, X.K.; Hao, Z.; Tan, S.K. Vortex-induced vibrations of a neutrally buoyant circular cylinder near a plane wall. *J. Fluids Struct.* **2013**, *39*, 188–204. [[CrossRef](#)]
- De Oliveira Barbosa, J.M.; Qu, Y.; Metrikine, A.V.; Lourens, E.M. Vortex-induced vibrations of a freely vibrating cylinder near a plane boundary: Experimental investigation and theoretical modelling. *J. Fluids Struct.* **2017**, *69*, 382–401. [[CrossRef](#)]
- Daneshvar, S.; Morton, C. On the vortex-induced vibration of a low mass ratio circular cylinder near a planar boundary. *Ocean Eng.* **2020**, *201*, 107109. [[CrossRef](#)]
- Khalak, A.; Williamson, C.H.K. Investigation of the relative effects of mass and damping in vortex-induced vibration of a circular cylinder. *J. Wind. Eng. Ind. Aerodyn.* **1997**, *69–71*, 341–350. [[CrossRef](#)]
- Sun, X.F.; Fang, X.S.; Guan, L.T. *Mechanics of Materials*, 5th ed.; Higher Education Press: Beijing, China, 2009.
- Sakai, T.; Oguma, N.; Morikawa, A. Microscopic and nanoscopic observations of metallurgical structures around inclusions at interior crack initiation site for a bearing steel in very high-cycle fatigue. *Fatigue Fract. Eng. Mater. Struct.* **2015**, *38*, 1305–1314. [[CrossRef](#)]
- Hong, Y.; Liu, X.; Lei, Z.; Sun, C. The formation mechanism of characteristic region at crack initiation for very-high-cycle fatigue of high-strength steels. *Int. J. Fatigue* **2016**, *89*, 108–118. [[CrossRef](#)]
- Avateffazeli, M.; Webster, G.; Tahmasbi, K.; Haghshenas, M. Very high cycle fatigue at elevated temperatures: A review on high temperature ultrasonic fatigue. *J. Space Saf. Eng.* **2022**, *9*, 488–512. [[CrossRef](#)]
- Sakai, T.; Nakagawa, A.; Oguma, N.; Nakamura, Y.; Ueno, A.; Kikuchi, S.; Sakaida, A. A review on fatigue fracture modes of structural metallic materials in very high cycle regime. *Int. J. Fatigue* **2016**, *93*, 339–351. [[CrossRef](#)]

32. Nadot, Y. Fatigue from defect: Influence of size, type, position, morphology and loading. *Int. J. Fatigue* **2022**, *154*, 106531. [[CrossRef](#)]
33. Schmiedel, A.; Henkel, S.; Kirste, T.; Morgenstern, R.; Weidner, A.; Biermann, H. Ultrasonic fatigue testing of cast steel G42CrMo4 at elevated temperatures. *Fatigue Fract. Eng. Mater. Struct.* **2020**, *43*, 2455–2475. [[CrossRef](#)]
34. Bayraktar, E.; Mora, R.; Garcia, I.; Bathias, C. Heat treatment, surface roughness and corrosion effects on the damage mechanism of mechanical components in the very high cycle fatigue regime. *Int. J. Fatigue* **2009**, *31*, 1532–1540. [[CrossRef](#)]
35. Gorash, Y.; Comlekci, T.; Styger, G.; Kelly, J.; Brownlie, F. Investigation of S275JR+AR structural steel fatigue performance in very high cycle domain. *Procedia Struct. Integr.* **2022**, *38*, 490–496. [[CrossRef](#)]
36. Palin-Luc, T.; Pérez-Mora, R.; Bathias, C.; Domínguez, G.; Paris, P.; Arana, J. Fatigue crack initiation and growth on a steel in the very high cycle regime with sea water corrosion. *Eng. Fract. Mech.* **2010**, *77*, 1953–1962. [[CrossRef](#)]
37. Pérez-Mora, R.; Palin-Luc, T.; Bathias, C.; Paris, P. Very high cycle fatigue of a high strength steel under sea water corrosion: A strong corrosion and mechanical damage coupling. *Int. J. Fatigue* **2015**, *74*, 156–165. [[CrossRef](#)]
38. Behvar, A.; Haghshenas, M. A critical review on very high cycle corrosion fatigue: Mechanisms, methods, materials, and models. *J. Space Saf. Eng.* **2023**, *10*, 284–323. [[CrossRef](#)]
39. Song, Q.Y. Observation of Characteristic and Analysis of Mechanism in Very High Cycle Fatigue Regime of High-Strength Steel. Ph.D. Thesis, University of Chinese Academy of Sciences, Beijing, China, 2021.
40. Lemos, M.; Kwietniewski, C.; Clarke, T.; Joia, C.J.B.; Altenhofen, A. Evaluation of the fatigue life of high-strength low-alloy steel girth welds in aqueous saline environments with varying carbon dioxide partial pressures. *J. Mater. Eng. Perform.* **2012**, *21*, 1254–1259. [[CrossRef](#)]
41. Gao, Z.; Gong, B.; Xu, Q.; Wang, D.; Deng, C.; Yu, Y. High cycle fatigue behaviors of API X65 pipeline steel welded joints in air and H₂S solution environment. *Int. J. Hydrogen Energy* **2021**, *46*, 10423–10437. [[CrossRef](#)]
42. Yan, Y.; Zhong, S.; Chen, Z.; Sun, Y.; Xu, L.; Zhao, L.; Han, Y. Corrosion fatigue behavior of X65 pipeline steel welded joints prepared by CMT/GMAW baking process. *Corros. Sci.* **2023**, *225*, 111568. [[CrossRef](#)]

Disclaimer/Publisher’s Note: The statements, opinions and data contained in all publications are solely those of the individual author(s) and contributor(s) and not of MDPI and/or the editor(s). MDPI and/or the editor(s) disclaim responsibility for any injury to people or property resulting from any ideas, methods, instructions or products referred to in the content.